Letter

Exploring the mass radius of ^{4}He and implications for nuclear structure

Rong Wang [*], Chengdong Han [†], and Xurong Chen [‡]

Institute of Modern Physics, Chinese Academy of Sciences, Lanzhou 730000, China
and School of Nuclear Science and Technology, University of Chinese Academy of Sciences, Beijing 100049, China

In this study, we determine the mass radius of ^{4}He, a very light nucleus, by examining the near-threshold ϕ-meson photoproduction data of the LEPS Collaboration. To assess the gravitational form factor of ^{4}He, we employ multiple models for the mass distribution, including Yukawa-type, exponential, Gaussian, and uniform functions. The mass radius of ^{4}He is measured to be 1.70 ± 0.14 fm, which is approximately equal to the charge radius of ^{4}He. Surprisingly, in contrast to the findings of the proton, no noticeable discrepancy between the charge radius and the mass radius is noted for the ^{4}He nucleus. The proton and neutron distributions within ^{4}He are likely to be identical, confirming its regular tetrahedral structure in a new way. We propose exploring the difference between charge and mass radii as a new approach to examine the nuclear structure.

DOI: 10.1103/PhysRevC.109.L012201

Introduction. The mass radius is an important and basic property for any composite system, from the subatomic particles of very small scale in high-energy physics to the galaxies of very large scale in astrophysics. The trace anomaly from the quantum corrections of quantum chromodynamics (QCD) breaks the conformal symmetry [1–3], and it is one key mechanism for the nucleon mass generation [4–10] and responsible for the most of the mass of the visible universe. The mass of a particle can be viewed as the response of the particle to an external gravitational field. The gravitational form factors (GFFs) of a particle are defined as the off-forward matrix elements of energy-momentum tensor (EMT) in the particle state [11–13]. The GFFs contain the fundamental properties of the particle, such as the mass and spin [12,13]. In the Breit frame, the 00 component of the static EMT is the energy density, and the energy density of the whole system should be normalized to the mass [13]. Therefore the mass density distribution and mass radius are all defined and derived from the GFFs.

The naive way to probe GFFs is via graviton scattering, however, it is infeasible due to the weakness of gravitational interaction of a particle. A practical opportunity is via the measurement of generalized parton distributions (GPDs) from various exclusive scattering processes. The second Mellin moments of GPDs yield the combinations of GFFs [12,13]. Recently, with some QCD analyses, it is suggested that the diffractive vector-meson photoproduction near the production threshold is sensitive to the gluonic GFFs of the target [14–24]. These QCD analyses result in three approaches for calculating the scattering amplitude of near-threshold vector-meson photoproduction: GPD approach [16,17], holographic QCD approach [18–22], and the factorization based on the vector-meson-dominance (VMD) model [14,15].

In experiment, the determination of mass radius is closely related to the extractions of GFFs from experimental data. Actually there are some pioneering works in determining the mass radii and GFFs of the proton [14,15,25], the deuteron [26], and the pion [27,28]. From these analyses, the mass radii of the studied hadronic particles are all smaller than the electric charge radii. With the recent experimental data of near-threshold J/Ψ photoproduction at Jefferson Lab (JLab), physicists have extracted the gluonic gravitational form factors of the proton with both the GPD approach and the holographic approach. They found that the mass radius is notably smaller than the charge radius, and the proton structure consists of three distinct regions [25].

In principle the concepts of mass radius and GFFs can be applied to a large hadronic system. At low energy, the nucleonic degree of freedom is valid for describing the static properties and low-energy reactions of an atomic nucleus. However, at high energy and a more fundamental level, the nucleus is built with quarks and gluons. It is very interesting to find out whether there is the difference between the mass radius and the charge radius of a nucleus. From our previous analysis, the mass radius of the loosely bound deuteron is slightly smaller than its charge radius [26]. However, for the tightly bound nucleus, such as the ^{4}He, we still lack the information on its mass radius and the related analysis.

The charge radius of ^{4}He is precisely measured to be 1.67824(83) fm with the technique of muon-atom spectroscopy [29], and the world average from electron elastic scattering experiments is 1.681(4) fm [30]. An older combined analysis gave the average charge radius of ^{4}He to be

1.6755(28) fm [31]. However, the mass radius of ^{4}He has never been studied. In this work, we investigate the mass radius of the helium nucleus from an analysis of the $|t|$ dependence of the differential cross section of near-threshold ϕ-meson photoproduction, which could provide important information about the gravitational properties and the internal structure of a large hadronic system, especially the transverse spatial distributions.

Near-threshold ϕ-meson photoproduction and gravitational form factors. The GFFs are the matrix elements of the EMT, which encode the mechanical properties of a composite particle. The trace anomaly of EMT sets up a mass scale of the hadronic system, and it is one key component of the origin of the proton mass according to the QCD analysis [4–10]. In the chiral limit, the scale anomaly is shown in the trace of EMT of QCD in terms of scalar gluon operator [14]. The trace anomaly in QCD is the pure quantum effect from gluon fluctuations. In Kharzeev's view, in the weak gravitational field, the trace of EMT and the temporal component of EMT T^{00} coincide [14]. The scalar GFF is then defined by Kharzeev as the form factor of the trace of the EMT. It is Lorentz invariant and defines the mass distribution of the system. In the chiral limit of massless quarks, the information about the mass radius of a hadronic system is contained in the matrix element of scalar gluon operator at a nonzero momentum transfer, for the matrix element does not depend on the strong coupling constant due to the scale anomaly [14].

In the nonrelativistic limit and based on the VMD model, the amplitude of a vector meson photoproduction can be safely factorized into a short-distance part describing the electric polarizability of the $q\bar{q}$ pair, and the matrix element of the chromoelectric operator over a hadron [14]. The scalar part in the chromoelectric operator is the trace of the EMT, and it dominates near the threshold of the vector-meson photoproduction as a consequence of scale anomaly. Therefore the vector-meson photoproduction amplitude can be expressed as [14],

$$\mathcal{M}_{\gamma p \to \phi p'}(t) = -Qec_2 \frac{16\pi^2 M}{b} \langle p'|T^\mu_\mu|p\rangle. \qquad (1)$$

The differential cross section is then computed with the square of the scattering amplitude, which is written as,

$$\frac{d\sigma_{\gamma p \to \phi p'}}{dt} = \frac{1}{64\pi s} \frac{1}{|E_{\gamma,\text{c.m.}}|^2} |\mathcal{M}_{\gamma p \to \phi p'}(t)|^2. \qquad (2)$$

With the above analysis and Eq. (1), the differential cross section is proportional to the square of the scalar GFF of the hadronic target, as,

$$\frac{d\sigma_{\gamma p \to \phi p'}}{dt} \propto |G(t)|^2. \qquad (3)$$

In some sense and the phenomenological view, the theoretical structures of the GFFs are similar in the processes probed by the graviton and the V^*V in the VMD model.

In this work, we study the $|t|$ dependence of the differential cross section of ϕ-meson photoproduction off the ^{4}He target with the theoretical framework in terms of the scalar GFF discussed above, in order to extract the mass radius of ^{4}He. For the convenience of discussions, we may define a normalized

TABLE I. Some density distributions, the corresponding form factors, and RMS radii.

Model	$\rho(r)$	$F(q)$	$\sqrt{\langle r^2 \rangle}$
Pointlike	$\frac{1}{4\pi r^2}\delta(r)$	1	0
Yukawa-type	$\frac{\Lambda^2}{4\pi r}e^{-\Lambda r}$	$\frac{1}{1+q^2/\Lambda^2}$	$\sqrt{\frac{6}{\Lambda^2}}$
Exponential	$\frac{\Lambda^3}{8\pi}e^{-\Lambda r}$	$\frac{1}{(1+q^2/\Lambda^2)^2}$	$\sqrt{\frac{12}{\Lambda^2}}$
Gaussian	$(\frac{\Lambda^2}{\pi})^{3/2}e^{-\Lambda^2 r^2}$	$e^{-q^2/(4\Lambda^2)}$	$\sqrt{\frac{3}{2\Lambda^2}}$
Uniform	$\frac{3}{4\pi R^3}\theta(R-r)$	$\frac{3j_1(qR)}{qR}$	$\sqrt{\frac{3R^2}{5}}$

scalar GFF $F(t)$ as,

$$F(t) = \frac{G(t)}{M}. \qquad (4)$$

The mass radius then can be simply computed with the slope of the scalar GFF at zero momentum transfer ($t = 0$ GeV^2), as,

$$\langle r_\text{m}^2 \rangle = -6\frac{dF(t)}{dt} = -\frac{6}{M}\frac{dG(t)}{dt}, \qquad (5)$$

which is also discussed in the following section. To be consistent with our previous analyses of the mass radii of the proton and the deuteron [15,26], we apply the same theoretical framework of the scalar GFF discussed above.

Various density distributions and form factors. The root-of-mean-square (RMS) radius $\sqrt{\langle r^2 \rangle}$ from a density distribution $\rho(r)$ is defined as,

$$\langle r^2 \rangle = \int_0^\infty r^2 \rho(r) 4\pi r^2 dr. \qquad (6)$$

In the low-momentum elastic scattering process, the form factor $F(q)$ of the target is measured, and it is the Fourier transformation of the density distribution $\rho(r)$. For a continuous density distribution and under the small momentum exchange, the RMS radius also can be easily computed with the slope of the form factor at $Q^2 = 0$ GeV^2, which is written as,

$$\langle r^2 \rangle = -6\frac{dF(q^2)}{dq^2}\bigg|_{q^2=0}. \qquad (7)$$

For different hadronic systems, the density distributions are different. The various and typical density distributions, the corresponding form factors and RMS radii are listed in Table I. For the light meson, such as the pion, the density reduces quickly with the increasing radial distance, and the density distribution is taken as the Yukawa potential form. The corresponding form factor of the pion is monopolelike. The dipole form factor from exponential distribution describes well the form factor of the proton in a wide kinematical range. For the heavy nucleus, such as the lead nucleus, the density distribution is approximately described with the uniform distribution or the Fermi distribution due to the saturation property of nuclear matter. The ^{4}He is a light and compact nucleus. The density distribution and the form factor of ^{4}He
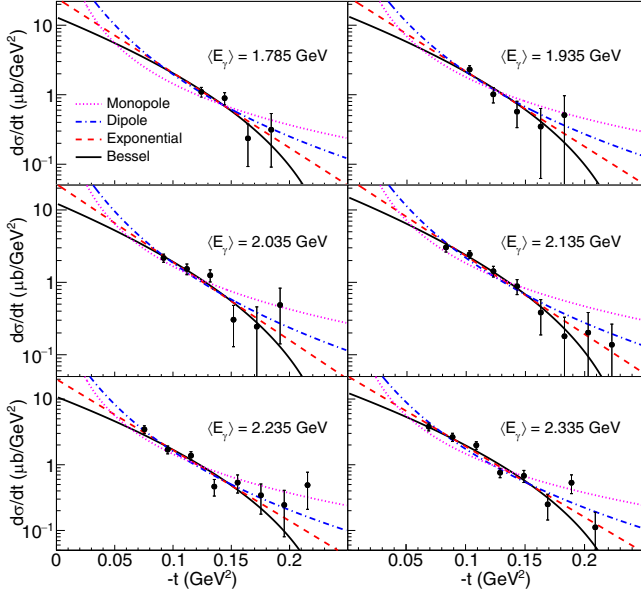
FIG. 1. The measured differential cross sections of the coherent ϕ-meson photoproduction off the ^{4}He nucleus near the threshold, compared with various models for the nuclear GFF. The experimental data are taken from LEPS Collaboration's publication [32]. The magenta dotted curves show the fitting results of the monopole GFF from Yukawa-type mass distribution. The blue dash-dotted curves show the fitting results of the dipole GFF from exponential mass distribution. The red dashed curves show the fitting results of the exponential GFF from Gaussian mass distribution. The black solid curves show the fitting results of the Bessel GFF from uniform mass distribution.

TABLE II. The determined model parameters, the extracted mass radii, and the fitting qualities $\chi^2/N_{\rm dof}$ with various models for the mass distribution.

Model	Λ (GeV)	$\sqrt{\langle r^2 \rangle}$ (fm)	$\chi^2/N_{\rm dof}$
Yukawa-type	0.045 ± 0.051	10.72 ± 12	$93.80/32$
Exponential	0.220 ± 0.063	3.10 ± 0.89	$40.98/32$
Gaussian	0.142 ± 0.011	1.70 ± 0.14	$34.09/32$
	R (GeV^{-1})		
Uniform	8.97 ± 0.47	1.37 ± 0.08	$37.50/32$

Nevertheless, the scalar GFF from Gaussian mass distribution most agree with the differential cross sections. More and precise experimental data in a large region of kinematic $|t|$ are needed to differentiate the models more clearly.

To quantify the quality of fit, the reduced χ^2 are calculated for different models, which are listed in Table II. One finds that the Gaussian mass distribution model describes the experimental data the best with the smallest $\chi^2/N_{\rm dof}$ quite close to 1.0. For describing a compact and small nucleus, the Gaussian distribution of the mass is a rather good choice. The uniform distribution of the mass also fits well the experimental data with $\chi^2/N_{\rm dof} < 1.2$. But the uniform mass distribution is just an overideal distribution for a heavy nucleus with the perfect nuclear saturation property.

The final results of the model fittings are summarized in Table II, including the extracted slope parameter Λ or R in the modeled GFFs, and the related mass radii. In the least-squares fit of each model, the slope parameter Λ (or R) of the GFF is the same for all the cross-section data at different photon energies. It is clearly shown that the extracted mass radii under different model assumptions vary significantly. There is a strong model dependence of the extracted mass radius. The first reason is that the $|t|$ range covered by the experimental data is narrow, about 0.15 GeV^2. The second reason is that the effective extrapolation of the slope to $t = 0$ GeV^2 requires more experimental data at small $|t|$ close to zero. On the other side, the model dependence is very natural in extraction of mass radius, since any model assumption definitely introduces the model uncertainty. Nonetheless, based on the current limited data, the exponential GFF of Gaussian mass distribution is the most effective model tested.

In the model fittings, the normalizations at different energies are set as free parameters, for we can not precisely or accurately compute them under the fundamental theory so far. Thus, including the parameter for modeling the scalar GFF, there are seven free parameters. As all the free parameters are important and have definite physical meanings, the multiparameter confidence region is considered in the analysis. Therefore we apply $\Delta\chi^2 = 8.38$ for the error estimations in multidimensional parameter space at the confidence level of 70%, suggested by the MINUIT manual.

Discussions and summary. From the analysis, we find that the differential cross section of near-threshold ϕ-meson photoproduction off the ^{4}He target can be described well at small $|t|$ with the exponential GFF of Gaussian mass distribution. The ^{4}He is a light nucleus, thus the uniform distribution is an inappropriate approximation for its mass distribution.

should be different from those of the proton and the heavy nucleus.

In this work, our goal is to determine the RMS mass radius of the ^{4}He nucleus from the coherent and diffractive scattering off the target. Thus the density distribution discussed above is specifically the mass distribution, and the form factor is the scalar GFF. To see which model of mass distribution and scalar GFF describes well the ^{4}He nucleus, the experimental data of the near-threshold ϕ-meson photoproduction off ^{4}He are fitted with various function forms of the scalar GFF.

Data analysis and results. Figure 1 shows the measured differential cross sections of the near-threshold ϕ-meson photoproductions as a function of t at different energies from LEPS Collaboration [32]. For the momentum transfer $\tilde{t}$ in the LEPS data, $|t|_{\rm min}$ is subtracted. In this analysis, we remove the correction on the momentum transfer by calculating the $|t|_{\rm min}$'s of the reaction $\gamma\,^4{\rm He} \rightarrow \phi\,^4{\rm He}$ at different photon energies. The differential cross sections are fitted with the models of various function forms for the scalar GFF. We investigated four different models: the monopole model, the dipole model, the Gaussian mass distribution model, and the uniform mass distribution model. In the data fitting with each model, the scalar GFF is the same for all the experimental data at different photon energies, and only the normalizations are different at different energies. One sees that all the models reproduce the experimental data in the narrow $|t|$ range.

Meanwhile the ^{4}He is a compact nucleus, its density in the center should not change fast with the radial distance increasing. This is probably why the Gaussian distribution model is most consistent with the measured differential cross sections.

For a heavy nucleus, the density is fairly a constant in the central region due the saturation property of nuclear force, and the density distribution can be approximately modeled with a uniform distribution, or the Fermi model with a radius parameter and a surface thickness [33,34]. For ^{12}C, the best fit of the electron elastic scattering data was found lying between a Gaussian model and a uniform model [33]. The latter studies found that the charge distributions of ^{12}C and ^{16}O can be described well with the harmonic-shell charge distributions [34]. For the charge distribution of the very light ^{4}He, it was found that the Gaussian model is the best in the low momentum transfer region (<6.2 fm^{-2}) [33–35]. The momentum transfer $|t|$ is below 6.2 fm^{-2} for the LEPS data used in this analysis. The pure Gaussian shape of charge distribution of ^{4}He is also provided by the shell model [34]. In this work, we find that the Gaussian distribution is also the best model in explaining the mass distribution of ^{4}He. The shapes of the mass and charge distributions are just alike for the nucleus.

The mass radius is obtained to be 1.70 ± 0.14 fm based on the Gaussian mass distribution model. The mass radius of the helium nucleus is nearly the same as its charge radius. This conclusion is quite surprising, as it violates what has been found for the proton [14,15,25], the deuteron [26], and the pion [27,28]. Why the mass radius of the proton is much smaller than its charge radius is a complicated and unanswered question. Why the mass radius of ^{4}He is almost the same of its charge radius is another astounding puzzle, which should be further investigated in the future experiments. One may simply assume the underlying confinement mechanisms for the proton and the nuclei are different, which should be carefully studied with the nonperturbative QCD theory in the future.

Figure 2 shows the differences and ratios between mass radius and charge radius, for some hadrons and nuclei examined recently. Based on the current analyses, the differences between mass and charge radii are similar for the pion and the proton, approximately 0.2 fm. Nonetheless, the difference in the mass and charge radii appears to vanish in ^{4}He. As the target size increases, the ratio of mass radius to charge radius goes up approaching one. In a picture of nucleonic degrees of freedom, the compatibility of the mass and charge radii of ^{4}He supports the regular tetrahedronlike structure of ^{4}He. Nuclear mass radius is related to both the proton and the neutron distributions inside a nucleus, whereas nuclear charge radius primarily connect to the proton distribution. Therefore, the radii of the proton distribution and the neutron distribution in ^{4}He are closely similar.

We argue that it is a pioneering and pivotal approach to scrutinize the nuclear structure via the examination of the difference between the charge and mass radii of a nucleus. For ^{9}Be of the dumbbell-like structure with a neutron at the center, its charge radius should obviously surpass its mass radius. For ^{208}Pb with the neutron skin on the crust, its charge radius is anticipated to be smaller than its mass radius. Extensive and systematical investigations on the mass and charge radii
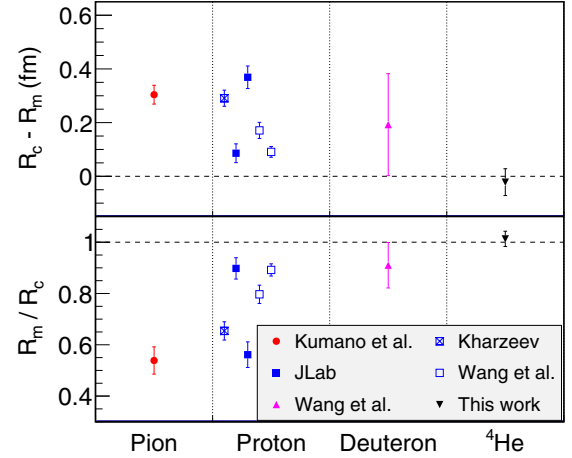

FIG. 2. The determined mass radii of the pion, the proton, the deuteron, and the ^{4}He nucleus, from various groups. The pion result is taken from Ref. [27]. The proton results are taken from Refs. [14,15,25]. The two values by JLab Hall C Collaboration are from the holographic QCD approach and the GPD approach. The two values by Wang *et al.* are from the analysis of only ϕ-photoproduction data and the combined analysis of the photoproductions of ω, ϕ, and J/ψ mesons. The deuteron result is taken from Ref. [26]. The helium result is from this work with the Gaussian mass distribution model.

of nuclei from different probes are highly promoted, which are essentially beneficial for solving the puzzles on the mass radius of ^{4}He and the complex structures of nuclei.

Lastly, our analysis reveals that different models produce very different extrapolation results on the mass radius, as shown by the disparate slopes approaching $t = 0$ GeV^2 in Fig. 1. To differentiate between the various forms of GFF for the light nucleus, we recommend experimental measurements across a wide kinematic range of $|t|$. In Fig. 3, we show the
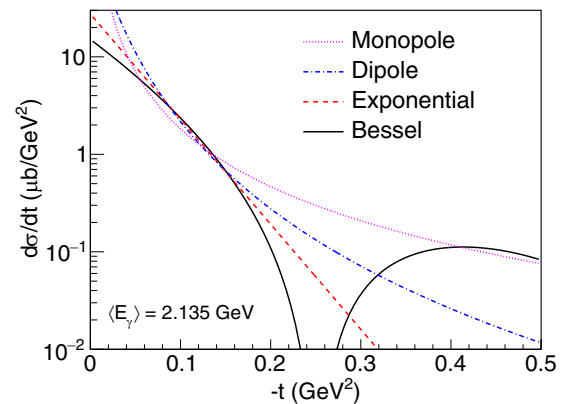

FIG. 3. The predictions of the differential cross section of ϕ-meson photoproduction near threshold in a broad t range with different models for the scalar GFF. The magenta dotted curve shows the prediction of monopole GFF. The blue dash-dotted curve shows the prediction of dipole GFF. The red dashed curve shows the prediction of exponential GFF. The black solid curve shows the prediction of Bessel-type GFF.

predicted differential cross sections for ϕ-meson photoproduction over a broad range of $|t|$ up to 0.5 GeV^2, based on the fitted scalar GFFs discussed earlier. The figures indicate that the shapes of the differential cross sections in different models vary significantly in the $|t|$ range above 0.2 GeV^2 or below 0.05 GeV^2. As the cross section decreases rapidly with increasing $|t|$, we will require high-luminosity experiments to collect coherent and diffractive data in the $|t|$ range from 0.2–0.5 GeV^2.

The US Electron-Ion Collider (EIC) under the ongoing construction [36,37] and the proposed Chinese Electron-Ion Collider (EicC) [38,39] show promises in achieving this goal by utilizing the plentiful quasireal photon flux. These facilities will offer an ample kinematical coverage and high statistics, and the high center-of-mass energies of the collisions will enable measurements of near-threshold heavy quarkonium (J/Ψ and Υ) photoproductions. Therefore, we recommend the comprehensive studies of near-threshold vector-meson photoproductions (ϕ, J/Ψ, and Υ) off nuclear targets at EIC and EicC. Such studies will differentiate between different scalar GFF models and reveal the puzzling mass radii and structures of the nuclei.

[1] N. K. Nielsen, Nucl. Phys. B **120**, 212 (1977).
[2] S. L. Adler, J. C. Collins, and A. Duncan, Phys. Rev. D **15**, 1712 (1977).
[3] J. C. Collins, A. Duncan, and S. D. Joglekar, Phys. Rev. D **16**, 438 (1977).
[4] X.-D. Ji, Phys. Rev. Lett. **74**, 1071 (1995).
[5] X.-D. Ji, Phys. Rev. D **52**, 271 (1995).
[6] X. Ji and Y. Liu, Sci. China Phys. Mech. Astron. **64**, 281012 (2021).
[7] X. Ji, Front. Phys. (Beijing) **16**, 64601 (2021).
[8] C. Lorcé, A. Metz, B. Pasquini, and S. Rodini, J. High Energy Phys. 11 (2021) 121.
[9] R. Wang, J. Evslin, and X. Chen, Eur. Phys. J. C **80**, 507 (2020).
[10] W. Kou, R. Wang, and X. Chen, Eur. Phys. J. A **58**, 155 (2022).
[11] H. Pagels, Phys. Rev. **144**, 1250 (1966).
[12] O. V. Teryaev, Front. Phys. (Beijing) **11**, 111207 (2016).
[13] M. V. Polyakov and P. Schweitzer, Int. J. Mod. Phys. A **33**, 1830025 (2018).
[14] D. E. Kharzeev, Phys. Rev. D **104**, 054015 (2021).
[15] R. Wang, W. Kou, Y.-P. Xie, and X. Chen, Phys. Rev. D **103**, L091501 (2021).
[16] Y. Guo, X. Ji, and Y. Liu, Phys. Rev. D **103**, 096010 (2021).
[17] L. Frankfurt and M. Strikman, Phys. Rev. D **66**, 031502(R) (2002).
[18] K. A. Mamo and I. Zahed, Phys. Rev. D **101**, 086003 (2020).
[19] Y. Hatta and D.-L. Yang, Phys. Rev. D **98**, 074003 (2018).
[20] Y. Hatta, A. Rajan, and K. Tanaka, J. High Energy Phys. 12 (2018) 008.
[21] Y. Hatta, A. Rajan, and D.-L. Yang, Phys. Rev. D **100**, 014032 (2019).
[22] K. A. Mamo and I. Zahed, Phys. Rev. D **106**, 086004 (2022).
[23] X. Ji, Y. Liu, and I. Zahed, Phys. Rev. D **103**, 074002 (2021).
[24] P. Sun, X.-B. Tong, and F. Yuan, Phys. Lett. B **822**, 136655 (2021).
[25] B. Duran *et al.*, Nature (London) **615**, 813 (2023).
[26] R. Wang, W. Kou, C. Han, J. Evslin, and X. Chen, Phys. Rev. D **104**, 074033 (2021).
[27] S. Kumano, Q.-T. Song, and O. V. Teryaev, Phys. Rev. D **97**, 014020 (2018).
[28] Y.-Z. Xu, K. Raya, Z.-F. Cui, C. D. Roberts, and J. Rodríguez-Quintero, Chin. Phys. Lett. **40**, 041201 (2023).
[29] J. J. Krauth *et al.*, Nature (London) **589**, 527 (2021).
[30] I. Sick, Phys. Rev. C **77**, 041302(R) (2008).
[31] I. Angeli and K. P. Marinova, At. Data Nucl. Data Tables **99**, 69 (2013).
[32] T. Hiraiwa *et al.* (LEPS Collaboration), Phys. Rev. C **97**, 035208 (2018).
[33] R. Hofstadter, Rev. Mod. Phys. **28**, 214 (1956).
[34] R. Hofstadter, Annu. Rev. Nucl. Sci. **7**, 231 (1957).
[35] R. F. Frosch, J. S. McCarthy, R. E. Rand, and M. R. Yearian, Phys. Rev. **160**, 874 (1967).
[36] R. Abdul Khalek *et al.*, Nucl. Phys. A **1026**, 122447 (2022).
[37] A. Accardi *et al.*, Eur. Phys. J. A **52**, 268 (2016).
[38] D. P. Anderle *et al.*, Front. Phys. (Beijing) **16**, 64701 (2021).
[39] X. Chen, F.-K. Guo, C. D. Roberts, and R. Wang, Few Body Syst. **61**, 43 (2020).